

The sounds of failure: forecasting granular slip events with passive acoustic measurements

Theodore A. Brzinski III* and Karen E. Daniels
Department of Physics, NC State University

Granular materials can fail through spontaneous events like earthquakes or brittle fracture. However, measurements and analytic models which forecast failure in this class of materials, while of both fundamental and practical interest, remain elusive. Materials including numerical packings of spheres, colloidal glasses, and granular materials have been known to develop an excess of low-frequency vibrational modes as the confining pressure is reduced. Here, we report experiments on sheared granular materials in which we monitor the evolving density of excited modes via passive monitoring of acoustic emissions. We observe a broadening of the distribution of excited modes coincident with both bulk and local plasticity, and clear evolution in the shape of the distribution before and after bulk failure. These results provide a new interpretation of the changing state of the material on its approach to stick-slip failure.

The framework provided by the jamming transition [1–3] has highlighted the extent to which granular and other amorphous systems share certain properties: spatially and dynamically heterogeneous response to stress, structural disorder, and inhomogeneous force transmission. While the onset of rigidity in jammed materials shares features with standard second-order phase transitions, jamming is differentiated from other such transitions by its lack of a diverging structural length-scale. Although jammed systems are not necessarily thermal, it has been observed that the density of vibrational modes $D(\omega)$ remains an important descriptor of the state of the system. In particular, an excess of low-frequency modes develops on approach to the jamming transition [4, 5] and the onset of plasticity [6]. Indeed, these excess low-frequency modes have been observed in experiments in colloidal systems [7, 8] as well as granular materials [9, 10].

As such, both experiments and simulations tantalizingly suggest that information about the rigidity of a system might be encoded within $D(\omega)$ as the system evolves under external loading. $D(\omega)$ is a particularly attractive metric since the passive recording of acoustic emissions provides a non-invasive method of reporting changes in the state of the system and does not require visual access to the system. For example, embedded sensors have long been used for non-destructive evaluation of engineered structures [11, 12], and have also successfully identified precursors in volcanic systems [13].

One practical method for measuring $D(\omega)$ has been to take advantage of the relationship between the particle velocity autocorrelation function and the density of vibrational modes [14, 15]. Recent experiments on a quasi-2D granular packing have used this relationship to establish a connection between acoustic modes and the jamming framework [10]. The procedure is to measure

the velocity autocorrelation function

$$C_v(\tau) \equiv \frac{\sum v_k(t+\tau)v_k(t)}{\sum v_k(t)v_k(t)}, \quad (1)$$

for $v_k(t)$ velocity timeseries measured using particle-scale piezoelectric sensors; the sums over k covers all sensors in the system. The density of vibrational modes is then given by [10]

$$D(\omega) = \int_0^\infty C_v(\tau) \cos(2\pi\omega\tau) d\tau. \quad (2)$$

This approach succeeds even for measurements over a small subset of the particles, recovering the expected Debye scaling for crystalline granular materials as well as the expected excess of low- ω modes in both amorphous and crystalline systems as the confining pressure was reduced.

Our experiments are inspired by prior work on slowly-loaded granular materials, from which it is known that (1) particle-scale rearrangements both precede and follow failure events [16], and (2) acoustic emissions and microslips show an exponential increase in their rate of occurrence leading up to a failure event [17, 18]. Here, we measure the acoustic emissions during the the lead-up to failure, and associate changes in the observed $D(\omega)$ with the approach to failure. In doing so, we provide a new means of acoustic monitoring. Unlike spectral power measurements, which capture the distribution of acoustic *power* among modes of different frequencies, the approach we introduce is effectively a measurement of the *number* of modes which are excited, regardless of the excitation amplitude. To differentiate from the true density of vibrational modes, we denote this measurement as the density of excited modes denoted as $D_{\text{ex}}(f)$, where f replaces ω as frequency.

Our experiment, depicted in Fig. 1a-c, comprises an annulus with an outer wall of diameter 66.75 cm and inner wall of diameter 30.5 cm. The system is filled with a single layer of approximately 8000 grains. The grains are a 60:40 mixture of 5.6 mm circular and 4.9

* tbrzinski@haverford.edu; Now at Department of Physics and Astronomy, Haverford College.

by 6.9 mm elliptical disks to prevent crystallization. All grains are milled from PhotoStress Plus PS-3 polymer from the Vishay Measurements Group with a bulk elastic modulus of 0.21 GPa. The granular material is sheared at a rate of 1 rotation per hour via a torsion spring (pictured in Fig. 1b) with a stiffness of 0.85 Nm/radian and a maximum compression of 26° , corresponding to a torque of 0.39 Nm. During an experiment, the driving torque (Fig. 1d) and acoustic emissions (Fig. 1e) of the system are continuously measured via a torque sensor (Cooper Instruments) and acoustic sensors (detailed in [19]).

This driving produces intermittent stick-slip failure events, apparent as the sawtooth features in Fig. 1d. The loading (stick) phase corresponds to the compression of the torsional spring, and when the applied torque surpasses the strength of the granular material, failure (slip) occurs. Empirically, after an initial transient, the frequency of slips remains close to 1 slip/minute. The data presented here were all collected in this steady state over the course of 23 hours. The full dataset of 1165 slip events are aperiodic and span a broad range of torque and time scales (see the inset in Fig. 1d), indicating strong heterogeneity in the material strength and degree of deformation. Despite the spatiotemporal heterogeneity, the slip durations exhibit a relatively narrow duration distribution with a mean of 0.65 ± 0.14 s. This slipping time scale is well-separated from the inter-slip (quiescent) timescale: more than 80% of slips, are preceded and followed by quiescent periods of 30 seconds or more. We focus our analysis on the subset of these 887 slips to isolate the effects of individual events.

An illustration of the typical intermittency of the acoustic emissions is provided in Fig. 1e; each trace is the power from one piezoelectric sensor. We observe that the largest emissions always coincide with slips. Importantly, the converse is not the case: not every slip produces a voltage spike in every sensor. This arises because the force chains cause spatial heterogeneities in acoustic transmission [19]. The typical RMS voltage during quiescent periods (without large torque drops) is 2.0 mV, the noise floor of our data acquisition hardware is 1.34 mV, and emission events can produce spikes as much as 3 orders of magnitude higher. In this paper we investigate the low-amplitude emissions during the largely quiescent periods between these slips.

In order to analyze the evolving state of the density of excited states, $D_{\text{ex}}(f; t - t_i)$, we follow the following procedure: For each piezoelectric sensor and slip event occurring at time t_i , we divide the voltage timeseries into 61 1 s intervals centered around t_i ; we calculate $D_{\text{ex}}(f)$ via Eqs. 1 & 2 [14, 15] (see Supp. Mat.); we plot this quantity as a function of frequency f and $t - t_i$ in *modograms*. Sample modograms for four events are shown in Fig. 2b. One prominent feature is that a broad range of modes is excited during each slip ($t = t_i$). However, similar increases in excited modes are also observed at times before and after the slips; these features are visible as bright vertical bands in Fig. 2b. In addition, we observe that the

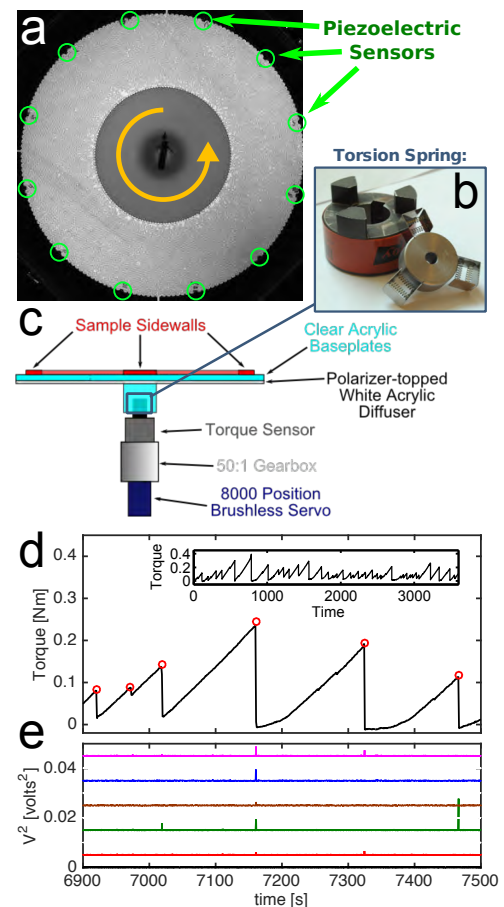


FIG. 1. (a) Top view of the annular shear cell, with piezoelectric sensors and moving (inner) wall. (b) Driveshaft coupling with Hookean torsion spring. (c) Schematic side view illustrating the details of the drive system. (d) Sample torque data over the course of 10 minutes and (inset) 1 hour. Red circles identify slips. (e) Sample measurements of the voltage squared, $V^2(t)$, measured for 5 piezoelectric sensors, vertically offset and plotted on the same time axis as (d).

overall density of excited modes appears to be relatively flat over nearly 3 decades (Hz to kHz), rising only at the highest frequencies in this range. Finally, we observe several persistent frequencies which appear as horizontal lines. While the 60 Hz peak is of electronic origin, the others are likely due to acoustic noise such as from the drive system or building noise. These noise peaks will be filtered out in the later stages of analysis.

We begin by focusing on the vertical bands visible in Fig. 2b. Each of these bands represents a time at which a single piezoelectric sensor detected an increase in the number of excited vibrational modes over a broad range of frequencies. Some of these vertical bands correspond to global slip events ($t = t_i$), but most are detected due to local rearrangements which happened to occur close to a particular sensor. The local nature of these detections is reinforced by the observation that modograms from different sensors do not all record in-

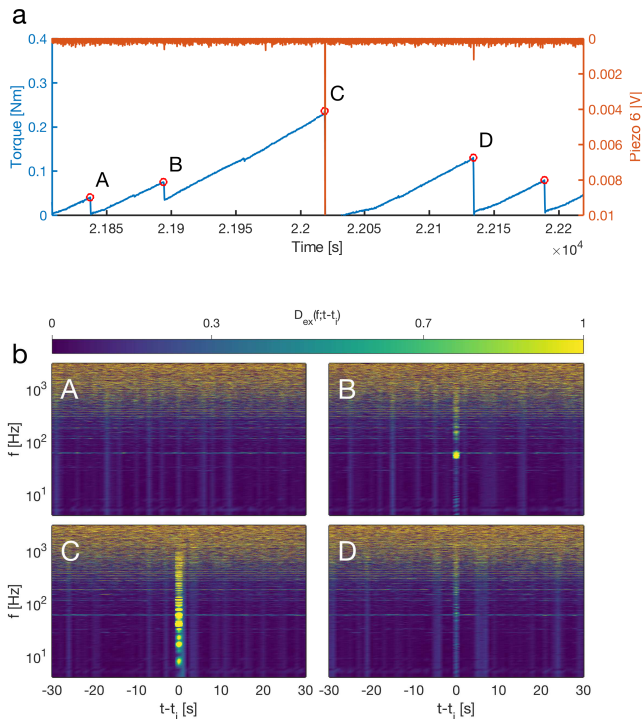


FIG. 2. (a) 400 s of torque (blue) and voltage (red) measurements from one piezoelectric sensor. 5 slips are labelled with red circles. (b) Sample modograms showing the density of excited modes $D_{\text{ex}}(f; t - t_i)$ for an interval of ± 30 s centered on each of the four labeled slips (A-D).

creases (as also seen in Fig. 1e). The ability to measure the $D_{\text{ex}}(f; t - t_i)$ from either low- or high-amplitude slip events is crucially-important to this method. While the low-amplitude events are too small to cause a global slip event, some of them are nonetheless large enough to be detected as they travel through the granular material and thereby leave a record of the state of the material. As we shall see below, the information they transmit reveals the changing state of the materials.

To reveal these small features, we can remove the background signal caused by the electronic/physical resonances. To do this, we construct the average modogram $\tilde{D}_{\text{ex}}(f; t - t_i) \equiv \langle D_{\text{ex}}(f; t - t_i) \rangle_{i,k}$, where i are the 887 detected slips separated by at least 30 s from the adjacent slips, and k are the 12 sensors. To remove the electronic/physical resonances we divide a background signal $B(f) = \langle \tilde{D}_{\text{ex}}(f; t - t_i) \rangle_{t \neq t_i}$ from $\tilde{D}_{\text{ex}}(f; t - t_i)$ to obtain the rescaled modogram shown in Fig. 3.

This average modogram exhibits features similar to the fluctuations observed in Fig. 2, but now the vertical streaks result from the average behavior over *many* slips and sensors. The remaining heterogeneity indicates that 887 slips was an insufficient quantity of data to eliminate the temporal heterogeneity associated with localized plasticity. Even within this noisy signal, however, there emerge clear differences between the pre- and post-slip portions of this modogram.

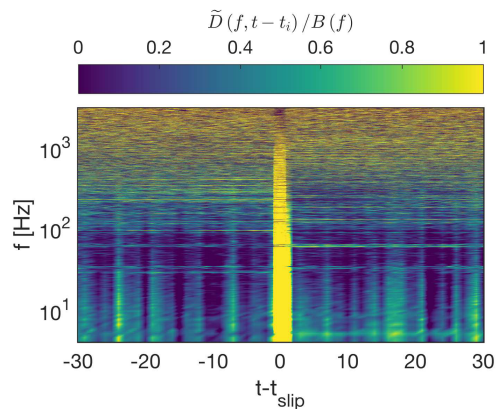


FIG. 3. Average modograms $\tilde{D}_{\text{ex}}(f; t - t_i)$, taken over 887 slips and 12 sensors and with the frequency-background $B(f)$ divided out.

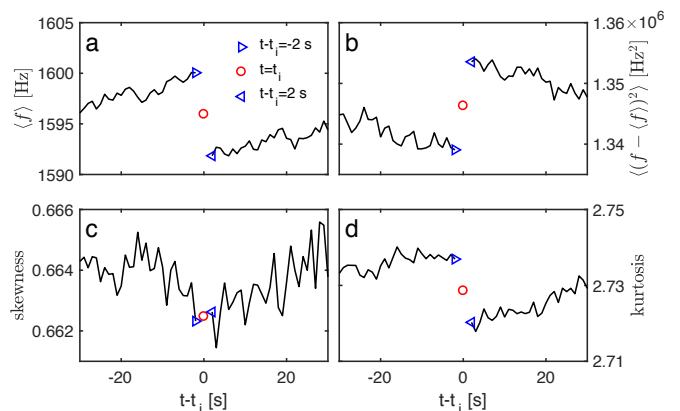
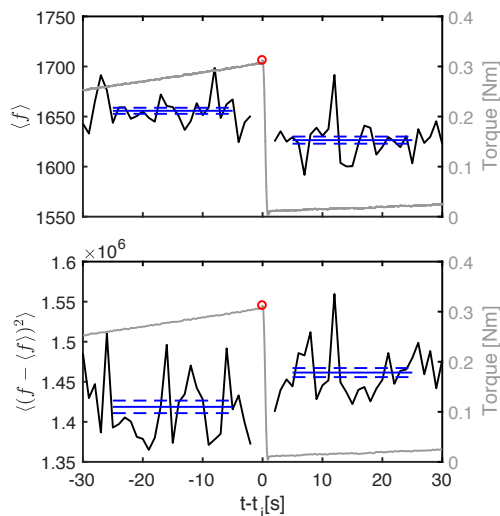


FIG. 4. The four moments of $\tilde{D}_{\text{ex}}(f; t - t_i)$, calculated at fixed times pre- and post-slip: (a) mean frequency, (b) variance, (c) skewness, and (d) kurtosis. The red ‘o’ indicates the time of the slip (datapoint omitted for clarity). The right- and left-pointing cyan triangles indicate the values immediately before and after the slip.

Evident in the four moments of the slip- and sensor-averaged $\tilde{D}_{\text{ex}}(f; t - t_i)$ (Fig. 4). We find that the mean frequency (a) gradually grows during the pre-slip phase, and then suddenly decreases from 1.60 to 1.59 kHz (less than 1%) in response to slips. This effect is accompanied by a small increase in the variance (b) These changes are consistent with a broadening of $\tilde{D}_{\text{ex}}(f)$ in response to failure, with additional modes arising at lower-frequencies. Since the internal stress in the granular material is lower after a slip (see Fig. 1d), these observations are consistent with the observations of failure of the force chain network [20] and emergence of excess low-frequency modes [10] at smaller confining stresses.

We also observe similarly clear, but still small, signals in the higher central moments of \tilde{D}_{ex} : a weak minima in skewness and a 1% drop in the kurtosis (panels c-d, respectively). We find a skewness of 0.66, which means low frequency modes are more common than high-frequency



| | Significant Rise | Significant Drop | Null |
|----------|------------------|------------------|------|
| mean | 9% | 34% | 57% |
| variance | 30% | 8% | 62% |
| kurtosis | 19% | 35% | 36% |

FIG. 5. (top) $\langle f \rangle$ and (middle) $\langle (f - \langle f \rangle)^2 \rangle$ for $D_{\text{ex}}(f; t - t_i)$ for a single slip, measured by a single sensor. The solid blue lines show the mean values for the first and last 28 seconds respectively, and dashed lines show the 95%-confidence in these means. In both plots, the torque is plotted on the right axis in light grey, with the slip indicated by a red circle. (bottom) The success rates for which we observed statistically significant discontinuities in the mean, variance and kurtosis in f for D_{ex} as measured by a single sensor and at a time coincident with a slip. Boldface values are those that match the sign of the average changes.

modes. The kurtosis close to 3 indicates \tilde{D}_{ex} is neither particularly heavy- nor weak-tailed.

Finally, we consider D_{ex} as a possible metric for characterizing single-slip, single-sensor measurements. In Fig. 5 we examine a characteristic example for a period centered on a single slip. $\langle f \rangle$ (top) and $\langle (f - \langle f \rangle)^2 \rangle$ (middle) of the excited modes, calculated based on a *single* sensor are plotted against $t - t_i$. To highlight the stepwise change at $t = t_i$, we additionally plot the mean $\pm 2\sigma$ as horizontal lines during the pre- and post-phases, and plot the torque on the right axis in both plots. As for the ensemble-averaged data (Fig. 4), we observe a significant drop in $\langle f \rangle$ coincident with the slip at $t = t_i$ accompanied by rise in the variance. We perform this same analysis for all slips that are well-separated in time, for all 12 piezos, for $887 \times 12 = 10644$ sets of statistics of the type shown in Fig. 5. The results of this analysis are summarized in the table in Fig. 5 (bottom). We find that single sen-

sor measurements are consistent with the trends depicted in Fig. 4, as emphasized by the boldface in Fig. 5 (bottom). Importantly, some slips will produce a detectable signal in these metrics for only one or a subset of sensors. Moreover, some slips produce no signal at any sensor due to the dissipative nature of the system and because the 12 sensors, each approximately 5 mm wide, cover less than 1% of the length of the perimeter.

The measurements we present here represent an important step in connecting passive acoustic measurements directly to the state of the material. While acoustic emissions have previously been known coincide with the failure of granular media, the method presented here provides a new capability: assessment of the progress of a system en route to failure. The shift observed in moments of the occupancy of vibrational modes is consistent with observations that granular systems under less stress exhibit an excess of floppy, low-frequency modes [10], and can be connected more broadly to similar observations in jammed solids as the volume fraction is reduced [7, 8, 21] and as shear progresses [22]. Our results indicate promise for predictive forecasting in systems with more complete sensor coverage, where passive measurements may more completely reveal the features of the density of vibrational modes. These techniques also provide a route for improved characterization of the vibrational properties of disordered materials.

Assessing the internal stress state of a granular system is notoriously difficult: photoelastic, optical, and tomographic techniques [23–25] require specialized materials or slow scanning times in order to make quantitative measurements of internal stresses. We have found that the density of excited vibrational modes $D_{\text{ex}}(f)$ appears to provide a new technique for reporting the internal stress in the system which does not require optical access, and can be applied to 3D systems with fast measurement times. Importantly, this method does not require acoustic-driving, which risks triggering a failure in materials near threshold, and should work on a variety of materials. Furthermore, this analysis is largely independent of the details of the sensor mechanism, so a clear next step is to test the approach with seismic data.

ACKNOWLEDGMENTS

This work was supported by NSF Grant DMR-1206808 and the James S. McDonnell Foundation. We thank Paul Johnson, Craig Maloney, Corey O’Hern and Eli Owens for helpful discussions, and Cross Automation for technical assistance with our motion control needs.

[1] A. J. Liu and S. R. Nagel, *Jamming and Rheology: Constrained Dynamics on Microscopic and Macroscopic*

Scales (CRC Press, 2001).

[2] A. J. Liu and S. R. Nagel, Annual Review of Condensed

- Matter Physics **1**, 347 (2010).
- [3] M. van Hecke, *J. Phys.: Cond. Matt.* **22**, 33101 (2010).
 - [4] C. S. O'Hern, L. E. Silbert, A. J. Liu, and S. R. Nagel, *Phys. Rev. E* **68** (2003), 10.1103/physreve.68.011306.
 - [5] M. Wyart, *Annales De Physique* **30**, 1 (2005).
 - [6] A. Tanguy, B. Mantsi, and M. Tsamados, *Europhysics Letters* **90**, 16004 (2010).
 - [7] A. Ghosh, V. K. Chikkadi, P. Schall, J. Kurchan, and D. Bonn, *Phys. Rev. Lett.* **104**, 248305 (2010).
 - [8] K. Chen, W. G. Ellenbroek, Z. Zhang, D. T. N. Chen, P. J. Yunker, S. Henkes, C. Brito, O. Dauchot, W. van Saarloos, A. J. Liu, and A. G. Yodh, *Phys. Rev. Lett.* **105**, 025501 (2010).
 - [9] C. Brito, O. Dauchot, G. Biroli, and J.-P. Bouchaud, *Soft Matter* **6**, 3013 (2010).
 - [10] E. T. Owens and K. E. Daniels, *Soft Matter* **9**, 1214 (2013).
 - [11] H. Dunegan, D. Harris, and C. Tatro, *Engineering Fracture Mechanics* **1**, 105 (1968).
 - [12] A. Nair and C. S. Cai, *Engineering Structures* **32**, 1704 (2010).
 - [13] G. Paparo, G. P. Gregori, U. Coppa, R. de Ritis, and A. Taloni, *Annals of Geophysics* **45**, 401 (2002).
 - [14] J. M. Dickey and A. Paskin, *Phys. Rev.* **188**, 1407 (1969).
 - [15] T. Keyes, *J. Phys. Chem. A* **101**, 2921 (1997).
 - [16] S. Nasuno, A. Kudrolli, and J. P. Gollub, *Phys. Rev. Lett.* **79**, 949 (1997).
 - [17] A. Garcimartín, A. Guarino, L. Bellon, and S. Ciliberto, *Phys. Rev. Lett.* **79**, 3202 (1997).
 - [18] P. A. Johnson, B. Ferdowsi, B. M. Kaproth, M. Scuderi, M. Griffa, J. Carmeliet, R. A. Guyer, P. Y. Le Bas, D. T. Trugman, and C. Marone, *Geophysical Research Letters* **40**, 5627 (2013).
 - [19] E. T. Owens and K. E. Daniels, *Europhysics Letters* **94**, 54005 (2011).
 - [20] D. Howell, R. P. Behringer, and C. Veje, *Phys. Rev. Lett.* **82**, 5241 (1999).
 - [21] L. E. Silbert, A. J. Liu, and S. R. Nagel, *Phys. Rev. Lett.* **95**, 098301 (2005).
 - [22] M. L. Manning and A. J. Liu, *Phys. Rev. Lett.* **107**, 108302 (2011).
 - [23] T. S. Majmudar and R. P. Behringer, *Nature* **435**, 1079 (2005).
 - [24] N. Brodu, J. A. Dijksman, and R. P. Behringer, *Nature Communications* **6**, 6361 (2015).
 - [25] R. Hurley, S. Hall, J. Andrade, and J. Wright, *Phys. Rev. Lett.* **117**, 098005 (2016).